Generation of acoustic waves by an impulsive line source in a fluid/solid configuration with a plane boundary

Adrianus T. de Hoop[a] and Jos H. M. T. van der Hijden
Schlumberger-Doll Research, P. O. Box 307, Ridgefield, Connecticut 06877

(Received 21 January 1983; accepted for publication 25 March 1983)

The space–time acoustic wave motion generated by a two-dimensional, impulsive, monopole line source in a fluid/solid configuration with a plane boundary is calculated with the aid of the modified Cagniard technique. The source is located in the fluid, and numerical results are presented for the reflected-wave acoustic pressure, especially in those regions of space where head wave contributions occur. There is a marked difference in time response in the different regimes that exist for the wave speed in the fluid in relation to the different wave speeds (compressional, shear, Rayleigh) in the solid. These differences are of importance to the situation where the reflected wave in the fluid is used to determine experimentally the elastic properties of the solid.

PACS numbers: 43.20.Px, 43.20.Rz, 43.25.Vt, 43.20.Fn, 43.20.Bi

INTRODUCTION

Acoustic waves as a diagnostic tool in determining the mechanical parameters (volume density of mass, compressibility, elastic stiffness) of fluids and solids have a widespread use. The applications range from geophysics (seismic exploration techniques, borehole soundings) to quantitative nondestructive evaluation of mechanical structures and acoustic tomography for medical purposes. In many cases, the theoretically obtained results for certain model configurations serve as a guidance when interpreting experimentally acquired data in the more complicated situations met in practice. To serve this purpose, the relative importance of the different parameters that govern the behavior of a certain configuration should show up as clearly as possible in the results that apply to the model configuration. Now, in any acoustic wave problem where fluid/solid interfaces play a role, the case of a plane boundary between the two serves as a canonical problem whose features should be thoroughly understood before analyzing more complicated geometries.

In the present paper, we investigate the acoustic wave motion in a fluid/solid configuration with a plane boundary. The source is taken to be a two-dimensional line source that emits an impulsive wave. In accordance with the situations met in borehole applications as well as in marine seismics, we locate the source in the fluid and compute the values of the acoustic pressure in the fluid.

The configuration considered here has been investigated before by Roever *et al.*[1] They investigate the three-dimensional point-source problem, but apply a two-dimensional type of approximation to evaluate the acoustic pressure in the fluid at large distances from the source. The latter two-dimensional problem is then solved with the aid of the original Cagniard technique. In the present paper, the problem is solved by applying the first author's modification of Cagniard's technique (de Hoop,[2–4] see also Achenbach,[5] Aki and Richards,[6] and Miklowitz[7]). The answer has a simple shape: just a convolution of the input signal of the source and the explicitly obtained space–time Green's function of the configuration. The space–time Green's function (or "system's response") clearly shows each feature of the time behavior of the acoustic pressure at different locations in dependence of the mechanical parameters involved. Also, the result can serve as a check on the accuracy of the numerical procedures that are used to evaluate the Fourier integrals in the standard spectral analysis of the problem, which seems to be the only available procedure in case the materials are lossy.

I. DESCRIPTION OF THE CONFIGURATION

We investigate theoretically the pulsed acoustic wave motion in a two-media configuration with a plane interface. One of the media is a homogeneous, ideal fluid; the other is a homogeneous, isotropic, perfectly elastic solid. The source is located in the fluid. It generates an impulsive wave motion that is reflected at the interface and, in this way, interacts with the solid. We determine expressions for the acoustic pressure of the reflected wave at any point in the fluid and at any time with the aid of the modified Cagniard technique. In the present paper, the two-dimensional case is considered.

To specify position in the configuration, we employ Cartesian coordinates $\{x_1 = x, x_2 = y, x_3 = z\}$ with respect

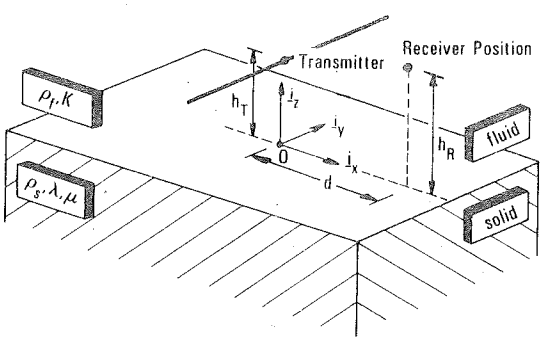

FIG. 1. Fluid/solid configuration with transmitter and receiver in fluid.

[a] Permanent address: Delft University of Technology, Department of Electrical Engineering, Laboratory of Electromagnetic Research, P. O. Box 5031, 2600 GA Delft, The Netherlands.

 0001-4966/83/070333-10$00.80

to a Cartesian reference frame with origin O and three mutually perpendicular base vectors of unit length $\{\mathbf{i}_1 = \mathbf{i}_x, \mathbf{i}_2 = \mathbf{i}_y, \mathbf{i}_3 = \mathbf{i}_z\}$. In the indicated order, the base vectors form a right-handed system. The z axis is chosen normal to the interface of the two media and the y axis is chosen parallel to the line source. The source strength of the latter is taken to be independent of y. The source, a transmitting transducer, is located at $x = 0$, $z = h_T$. The receiver, a receiving transducer, is located at $x = d$, $z = h_R$. The further properties of the configuration are listed in Table I (see also Fig. 1).

The time coordinate is denoted by t. It is assumed that the source starts to act at the instant $t = 0$ and that prior to this instant the entire configuration is at rest.

Since the strength of the source and the properties of the configuration are both independent of y, the total acoustic wave motion will be independent of y and hence all derivatives with respect to y vanish in the partial differential equations that govern the wave motion.

II. DESCRIPTION OF THE WAVE MOTION IN THE CONFIGURATION

In the fluid, the acoustic wave motion consists of the superposition of the incident wave and the reflected wave. The incident wave is the wave that would be generated by the transmitting transducer if the fluid were of infinite extent; it will be denoted by the superscript "i." The reflected wave is the difference between the actual wave motion in the fluid and the incident wave; it will be denoted by the superscript "r." In the fluid we consider the acoustic pressure p as the fundamental unknown quantity and hence we have

$$p = p^i + p^r \text{ in the domain } D_f. \tag{1}$$

The transmitted wave in the solid consists of a P wave that travels with speed c_P and whose particle displacement $\mathbf{u}^P$ is curlfree, and an S wave that travels with speed c_S and whose particle displacement is divergencefree. In the solid we consider the particle displacement $\mathbf{u}$ as the fundamental unknown quantity and hence we have

$$\mathbf{u} = \mathbf{u}^P + \mathbf{u}^S \text{ in the domain } D_s. \tag{2}$$

In the modified Cagniard technique we first calculate the wave constituents in the transformed domain, i.e., after having carried out a one-sided Laplace transform with respect to time, with real, positive transform parameter s, and a two-sided Laplace transform with respect to the coordinate x parallel to the interface, with purely imaginary transform parameter sp. (In subsequent calculations, the expressions will be continued analytically into the complex p plane, away from the imaginary axis.) To show the notation, we write down the relevant transforms for the acoustic pressure:

$$\hat{p}(x, z, s) = \int_0^\infty \exp(-st)p(x, z, t)dt, \tag{3}$$

$$\tilde{p}(p, z, s) = \int_{-\infty}^{\infty} \exp(sp\,x)\hat{p}(x, z, s)dx, \quad \text{with } \mathrm{Re}(p) = 0, \tag{4}$$

$$\hat{p}(x, z, s) = \left(\frac{s}{2\pi i}\right)\int_{-i\infty}^{i\infty} \exp(-sp\,x)\tilde{p}(p, z, s)dp. \tag{5}$$

In Eq. (5) we have taken into account, that in Eq. (4) the transform parameter is sp.

A. Incident wave

We now consider, more specifically, the case where the line source is a monopole source. Accordingly, we have

$$\tilde{p}^i = A^i \exp(-s\gamma_f|z - h_T|), \tag{6}$$

where

$$\gamma_f = (1/c_f^2 - p^2)^{1/2} \text{ with } \mathrm{Re}(\gamma_f) \geqslant 0, \tag{7}$$

and

$$A^i = s^2\rho_f\hat{\phi}_V/2s\gamma_f, \tag{8}$$

where $\hat{\phi}_V$ is given by

$$\hat{\phi}_V = \int_0^\infty \exp(-st)\phi_V(t)dt, \tag{9}$$

the monopole source being characterized by a volume density of injected fluid volume of the type

$$\Phi_V = \phi_V(t)\delta(x, z - h_T). \tag{10}$$

Hence, $\phi_V(t)$ represents the pulse shape of the source signal. In the calculations we further need the z component of the particle displacement. This follows from the equation of motion and the expression Eq. (6) as

$$\tilde{u}_z^i = \pm(\gamma_f/s\rho_f)A^i \exp(-s\gamma_f|z - h_T|) \quad \text{when } z \gtrless h_T. \tag{11}$$

B. Reflected wave

For the reflected wave we write

$$\tilde{p}^r = A^r \exp[-s\gamma_f(z + h_T)] \quad \text{in the domain } D_f. \tag{12}$$

To express the linear relationship between A^r and A^i we introduce the reflection coefficient R_f for the reflected wave in the fluid through

$$A^r = R_f A^i. \tag{13}$$

The z component of the particle displacement associated with the reflected wave then follows as

$$\tilde{u}_z^r = (\gamma_f/s\rho_f)A^r \exp[-s\gamma_f(z + h_T)] \quad \text{in the domain } D_f. \tag{14}$$

TABLE I. Properties of the fluid/solid configuration.

	Fluid	Solid
Domain	D_f	D_s
z coordinate	$0 < z < \infty$	$-\infty < z < 0$
Volume density of mass	ρ_f	ρ_s
Constitutive parameter(s)	K (bulk modulus of compression)	λ, μ (Lamé coefficients)
Wave speed(s)	$c_f = (K/\rho_f)^{1/2}$	$c_P = [(\lambda + 2\mu)/\rho_s]^{1/2}$ $c_S = (\mu/\rho_s)^{1/2}$

C. Transmitted P wave

The transform-domain representation of the transmitted P wave is written as

$$\{\tilde{u}_x^P, \tilde{u}_z^P\} = \{p, -\gamma_P\} A^P \exp[s(\gamma_P z - \gamma_f h_T)] \quad \text{in the domain } D_s, \tag{15}$$

where

$$\gamma_P = (1/c_P^2 - p^2)^{1/2} \text{ with } \mathrm{Re}(\gamma_P) \geqslant 0. \tag{16}$$

Equation (15) expresses that the P wave travels with speed c_P and that its particle displacement is curlfree. To express the linear relationship that exists between A^P and A^i, we introduce the P-wave particle displacement transmission coefficient T_P through

$$A^P = (c_P/s\rho_f c_f) T_P A^i. \tag{17}$$

In the calculations we further need the x, z and z, z components of the stress in the solid. They follow upon substituting the expression for the particle displacement in the constitutive relation. For the P wave they follow as

$$\{\tilde{\tau}_{x,z}^P, \tilde{\tau}_{z,z}^P\} = 2\mu s\{p\gamma_P, p^2 - 1/2c_S^2\} A^P \exp[s(\gamma_P z - \gamma_f h_T)] \quad \text{in the domain } D_s. \tag{18}$$

D. Transmitted S wave

The transform-domain representation of the transmitted S wave is written as

$$\{\tilde{u}_x^S, \tilde{u}_z^S\} = \{-\gamma_S, -p\} A^S \exp[s(\gamma_S z - \gamma_f h_T)] \quad \text{in the domain } D_s, \tag{19}$$

where

$$\gamma_S = (1/c_S^2 - p^2)^{1/2} \text{ with } \mathrm{Re}(\gamma_S) \geqslant 0. \tag{20}$$

Equation (19) takes into account that the S wave travels with speed c_S and that its particle displacement is divergencefree. To express the linear relationship that exists between A^S and A^i, we introduce the S-wave particle displacement transmission coefficient T_S through

$$A^S = (c_S/s\rho_f c_f) T_S A^i. \tag{21}$$

For the S wave, the x, z and z, z components of the stress follow as

$$\{\tilde{\tau}_{x,z}^S, \tilde{\tau}_{z,z}^S\} = 2\mu s\{p^2 - 1/2c_S^2, -p\gamma_S\} A^S \exp[s(\gamma_S z - \gamma_f h_T)] \quad \text{in the domain } D_s. \tag{22}$$

With this, the transform-domain description of the wave motion in the configuration has been completed. In the next section, we determine the as yet unknown reflection and transmission coefficients R_f, T_P, and T_S by applying the boundary conditions at the fluid/solid interface.

III. DETERMINATION OF THE REFLECTION AND TRANSMISSION COEFFICIENTS

The boundary conditions at the fluid/solid interface require the continuity of the normal component of the particle displacement, the equality of the normal component of the traction in the solid and the opposite of the acoustic pressure in the fluid, and the vanishing of the tangential component(s) of the traction in the solid. In the transform domain, these conditions lead to the equations

$$\lim_{z \uparrow 0} (\tilde{u}_z^P + \tilde{u}_z^S) = \lim_{z \downarrow 0} (\tilde{u}_z^i + \tilde{u}_z^r), \tag{23}$$

$$\lim_{z \uparrow 0} (\tilde{\tau}_{z,z}^P + \tilde{\tau}_{z,z}^S) = \lim_{z \downarrow 0} (-\tilde{p}^i - \tilde{p}^r), \tag{24}$$

$$\lim_{z \uparrow 0} (\tilde{\tau}_{x,z}^P + \tilde{\tau}_{x,z}^S) = 0. \tag{25}$$

Substitution of the relevant expressions in these equations leads to

$$R_f = (-\rho_f \gamma_P/4\rho_s \gamma_f c_S^4 + \Delta_R)/\Delta_{\mathrm{SCH}}, \tag{26}$$

$$T_P = -(\rho_f c_f/\rho_s c_P)(p^2 - 1/2c_S^2)/c_S^2 \Delta_{\mathrm{SCH}}, \tag{27}$$

$$T_S = (\rho_f c_f/\rho_s c_S) p\gamma_P/c_S^2 \Delta_{\mathrm{SCH}}, \tag{28}$$

where

$$\Delta_R = (p^2 - 1/2c_S^2)^2 + p^2 \gamma_P \gamma_S \tag{29}$$

is the "Rayleigh-wave denominator" and

$$\Delta_{\mathrm{SCH}} = \rho_f \gamma_P/4\rho_s \gamma_f c_S^4 + \Delta_R \tag{30}$$

is the "Scholte-wave denominator." The Rayleigh-wave denominator is associated with surface waves along a traction-free boundary of a solid (Rayleigh,[8] see also Achenbach[9]). The Scholte-wave denominator is associated with surface waves along a fluid/solid interface (Scholte,[10,11] see also Cagniard,[12] and Miklowitz[13]).

With this, the transform-domain expressions for the wave motion in the configuration have been fully determined. The transformation of these expressions to the space–time domain is carried out in subsequent sections. Explicit results will be given for the acoustic pressure of the reflected wave in the fluid, since in all practical applications this quantity is directly accessible to measurement.

IV. SPACE–TIME DOMAIN EXPRESSION FOR THE ACOUSTIC PRESSURE OF THE REFLECTED WAVE

Considering the fluid/solid configuration as a linear system in which, through the reflected wave, signals upon their way from the transmitting transducer to the receiving transducer gather information about the solid to be "sounded," we would like to write the time Laplace transform expression $\hat{p}^r$ for the acoustic pressure of the reflected wave as [cf. Eqs. (6) and (8)]

$$\hat{p}^r = s^2 \rho_f \hat{\phi}_V \hat{G}_f^r, \tag{31}$$

where $\hat{G}_f^r$ is the time Laplace transform of the space–time Green's function for the reflected wave in the fluid. Once the corresponding space–time Green's function G_f^r has been determined, we can write the space–time expression p^r for the acoustic pressure of the reflected wave as

$$p^r(\cdot, t) = \rho_f \partial_t^2 \int_0^t \phi_V(t - \tau) G_f^r(\cdot, \tau) d\tau, \quad \text{when } 0 < t < \infty. \tag{32}$$

In Eq. (32), the dot in the argument stands for the spatial variables. Now, the space and time Laplace transformed equivalent of Eq. (31) would be

$$\tilde{p}^r = s^2 \rho_f \hat{\phi}_V \tilde{G}_f^r. \tag{33}$$

Comparing Eq. (33) with Eqs. (12), (13), and (8), we arrive at

$$\tilde{G}_f^r = (R_f/2s\gamma_f)\exp[-s\gamma_f(z+h_T)], \tag{34}$$

in which R_f is given by Eq. (26). Starting from Eq. (34), the expression for G_f^r is obtained with the aid of the modified Cagniard technique. This technique accomplishes the transformation of the p-plane integration [cf. Eq. (5)]

$$\hat{G}_f^r = \left(\frac{s}{2\pi i}\right)\int_{-i\infty}^{i\infty}\left(\frac{R_f}{2s\gamma_f}\right)\exp\{-s[px+\gamma_f(z+h_T)]\}dp \tag{35}$$

into the real integration

$$\hat{G}_f^r(\cdot,s) = \int_T^\infty \exp(-s\tau)\Gamma(\cdot,\tau)d\tau, \tag{36}$$

where $\Gamma(\cdot,\tau)$ is an expression that does not depend on s, and where the dot stands for the spatial variables. The uniqueness theorem of the Laplace transform with real, positive transform parameter s then ensures that (Lerch's theorem, see Widder[14])

$$G_f^r(\cdot,\tau) = \begin{cases} 0 & \text{when } -\infty < \tau < T, \\ \Gamma(\cdot,\tau) & \text{when } T < \tau < \infty. \end{cases} \tag{37}$$

Here, T apparently is the arrival time of the reflected wave. The actual transformation follows the pattern of the modified Cagniard technique for two-dimensional wave motion. The final result is obtained as

$$G_f^r = \begin{cases} 0 & \text{when } -\infty < \tau < T_{fP}, \\ \mathrm{Im}[R_f(p^{fP})]/2\pi(T_{ff}^2 - \tau^2)^{1/2} & \text{when } T_{fP} < \tau < T_{ff}, \\ \mathrm{Re}[R_f(p^{ff})]/2\pi(\tau^2 - T_{ff}^2)^{1/2} & \text{when } T_{ff} < \tau < \infty, \end{cases} \tag{38}$$

where

$$T_{fP} = d/c_P + (1/c_f^2 - 1/c_P^2)^{1/2}(h_T + h_R) \tag{39}$$

is the arrival time of the head wave or lateral wave (if present),

$$T_{ff} = [d^2 + (h_T + h_R)^2]^{1/2}/c_f \tag{40}$$

is the arrival time of the reflected body wave in the fluid,

$$p^{fP} = \frac{d\tau - (h_T + h_R)(T_{ff}^2 - \tau^2)^{1/2} + i0}{d^2 + (h_T + h_R)^2} \quad \text{with } T_{fP} < \tau < T_{ff} \tag{41}$$

is the mapping from τ onto p for the head-wave contribution,

$$p^{ff} = \frac{d\tau + i(h_T + h_R)(\tau^2 - T_{ff}^2)^{1/2}}{d^2 + (h_T + h_R)^2} \quad \text{with } T_{ff} < \tau < \infty \tag{42}$$

is the mapping from τ onto p for the fluid body-wave contribution,

d = transmitter-to-receiver spacing measured along the interface,

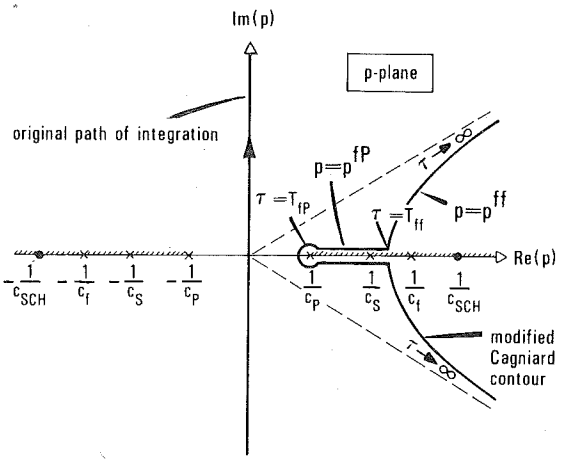

FIG. 2. Complex p plane with singularities of R_f and γ_f and modified Cagniard contours; the case $c_f < c_P$ is shown, while $c_S < c_P$.

h_T = distance from transmitter to interface,

h_R = distance from receiver to interface.

The head-wave contribution is only present in those regions in space where $d/[d^2 + (h_T + h_R)^2]^{1/2} > c_f/c_P$. In arriving at Eq. (38), we have assumed the case most often met in practice where $c_f < c_P$. Note, that for any solid we have $c_S < c_P$. The results hold for the two cases that remain as far as c_f is compared with c_S, viz., $c_f < c_S$, and $c_f > c_S$ ("fast formation" and "slow formation," respectively, for geoscience applications). In case $c_P < c_f$, the head-wave contribution in Eq. (38) is absent.

Numerical results based upon Eq. (38) will be presented in the next section. The typical features of the thus obtained "computer seismogram" can all be attributed to the singularities of R_f in the complex p plane, cut in accordance with the conditions put on the square-root expressions in Eqs. (7), (16), and (20). These are: the two branch points $p = \pm 1/c_f$ due to γ_f, the two branch points $p = \pm 1/c_P$ due to γ_P, the two branch points $p = \pm 1/c_S$ due to γ_S, and the two simple poles on the real axis (Scholte poles) $p = \pm 1/c_{\mathrm{SCH}}$, where

$$\Delta_{\mathrm{SCH}}(p) = 0 \text{ at } p = \pm 1/c_{\mathrm{SCH}}. \tag{43}$$

It can be proved that $c_{\mathrm{SCH}} < \min(c_f, c_P, c_S)$, while for solids with positive Poisson ratio we always have $c_S < c_P/2^{1/2}$. Further, in order to keep R_f and γ_f single valued, we introduce, in accordance with the conditions put on the square-root expressions in Eqs. (7), (16), and (20), branch cuts along $1/c_f < |\mathrm{Re}(p)| < \infty$, $\mathrm{Im}(p) = 0$; $1/c_P < |\mathrm{Re}(p)| < \infty$, $\mathrm{Im}(p) = 0$; and $1/c_S < |\mathrm{Re}(p)| < \infty$, $\mathrm{Im}(p) = 0$. For the case most often met in practice, where $c_f < c_P$, the situation is shown in Fig. 2.

In this situation, the branch point $p = 1/c_P$ is the first singularity we meet upon deforming the path of integration from the imaginary p axis to the modified Cagniard contour.

With the aid of the principle of the argument it can further, by an elaborate calculation, be shown that in the cut complex p plane R_f has two simple poles and four simple zeros (see the Appendix). If $\rho_f/\rho_s = (2c_S^2/c_f^2 - 1)^{1/2}$, the zeros are located on the branch cut at $p = \pm 1/c_S\sqrt{2} \pm i0$.

V. NUMERICAL RESULTS

In this section, we present some curves showing computed space–time Green's functions. Five different regimes are distinguished. We make a choice as to the parameters of the solid. Then, four characteristic points on the real p axis (Fig. 2) are already fixed: $1/c_P$, $1/c_S\sqrt{2}$, $1/c_S$, and $1/c_R$, where $\Delta_R(p) = 0$ at $p = \pm 1/c_R$. Next, we subsequently choose $1/c_f$ in the five regions that are generated by these four points. The parameters that are kept fixed are listed in Table II. The subsequent choices for the remaining parameter are listed in Table III.

In Figs. 3–7, the space–time Green's function is plotted as a function of time for three different transmitter/receiver distances, viz., $d = 0.2$, 0.4, and 0.6 m, while in all cases $h_T = h_R = 0.01$ m.

A. Interval $0 < c_f < c_R$

In Fig. 3 results are presented for a fast formation. The arrival times of the different wave types are marked by arrows. At $t = T_{fP}$, the arrival time of the compressional head wave, the Green's function has a discontinuity in slope. For the limiting values we have

$$\lim_{t \downarrow T_{fP}} \partial_t G_f^r = 0 \text{ and } \lim_{t \downarrow T_{fP}} \partial_t G_f^r = \infty. \tag{44}$$

At $t = T_{fS}$, the arrival time of the shear head wave, which is defined by Eq. (39), if we replace c_P by c_S, the Green's function again has a vertical tangent. At $t = T_{ff}$, the reflected fluid wave arrival time, the Green's function becomes negative infinite because of the square root singularity occurring in the wave emitted by a two-dimensional line source [see Eq. (38)]. Finally, at the Scholte wave arrival time $t = T_{\mathrm{SCH}}$, defined by $T_{\mathrm{SCH}} = d/c_{\mathrm{SCH}}$, the Green's function has the polelike behavior with a rapid change in sign. Apart from the behavior around these arrival times, there are some other features that we want to mention. In the interval between T_{fP} and T_{fS} the Green's function has a zero with zero slope at the time [cf. Eqs. (39) and (A26)]

$$t = d/\sqrt{2}c_S + (1/c_f^2 - 1/2c_S^2)^{1/2}(h_T + h_R). \tag{45}$$

Further, in the interval between T_{fS} and T_{ff} there is a zero crossing exactly at the time defined by

$$T_{fR} = d/c_R + (1/c_f^2 - 1/c_R^2)^{1/2}(h_T + h_R). \tag{46}$$

This follows from Eqs. (38) and (26), observing the fact that Δ_R vanishes at $t = T_{fR}$, and hence, $R_f = -1$, a real value. The bump in the signal in the interval between T_{fS} and T_{fR} is due to the pseudo-Rayleigh phenomenon and will be discussed extensively in a separate paper.

TABLE II. Numerical values of the parameters that are kept fixed (parameters of the solid and volume density of mass of the fluid).

Parameter	Value
c_P	3500 m/s
c_S	2000 m/s
$c_S\sqrt{2}$	2828 m/s
c_R	1841 m/s
ρ_s	2500 kg/m^3
ρ_f	1000 kg/m^3

TABLE III. Numerical values of the remaining parameter (fluid speed) in the different regimes.

Interval of c_f	c_f(m/s)	c_{SCH}(m/s)
$0 < c_f < c_R$	1500	1436
$c_R < c_f < c_S$	1920	1613
$c_S < c_f < c_S\sqrt{2}$	2400	1669
$c_S\sqrt{2} < c_f < c_P$	3150	1695
$c_P < c_f < \infty$	4000	1706

B. Interval $c_R < c_f < c_S$

The results for this regime are presented in Fig. 4. The major difference with the previous regime is that the zero crossing at T_{fR} is not present anymore. Further, at T_{fS}, the Green's function still has a vertical tangent but now there also is a discontinuity in slope. Finally, there is a tendency (that will continue in the subsequent intervals) for the Scholte wave to become less pronounced and more separated in time from the reflected fluid wave arrival.

C. Interval $c_S < c_f < c_S\sqrt{2}$

In Fig. 5, the Green's function for a slow formation is shown. It is clear that the shear head wave arrival is not present anymore.

D. Interval $c_S\sqrt{2} < c_f < c_P$

In this case, shown in Fig. 6, also the double zero in the interval between T_{fP} and T_{fS} has disappeared.

E. Interval $c_P < c_f < \infty$

Figure 7 shows that in this case the fluid arrival and weak Scholte wave are the only features left in the space–time Green's function.

The time required to compute the Green's functions for one of the previous figures on a VAX 11/780 computer amounts to about 5 s.

In Fig. 8, we present a synthetic seismogram for the received acoustic pressure, in case the space–time Green's function has been convolved with a certain source pressure pulse. For the pulse shape of the source, we have used a four-point optimum Blackman window function, i.e.,

$$\rho_f \phi_V(t) = \begin{cases} 0 & \text{when } -\infty < t < 0, \\ \sum_{n=0}^{3} b_n \cos\left(\dfrac{2\pi n t}{T}\right) & \text{when } 0 < t < T, \\ 0 & \text{when } T < t < \infty, \end{cases} \tag{47}$$

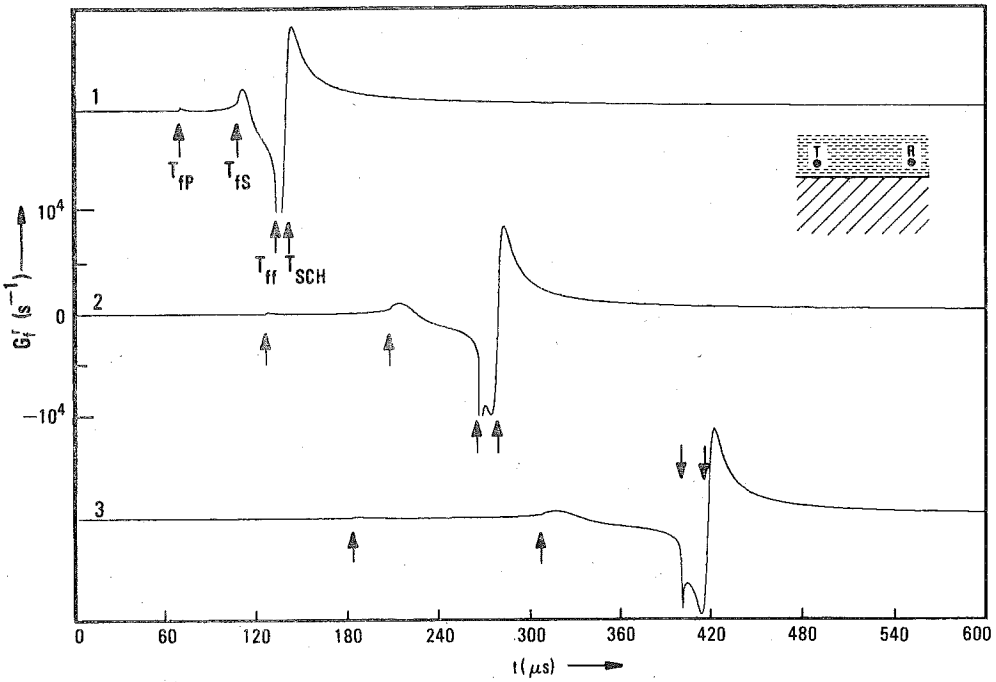

FIG. 3. Space–time Green's function G_f^r for the reflected acoustic pressure in a fluid from a fluid/solid interface as a function of time for three transmitter/receiver distances: (1) $d = 0.2$ m, (2) $d = 0.4$ m, (3) $d = 0.6$ m. Further, $c_P = 3500$ m/s, $c_S = 2000$ m/s, $c_f = 1500$ m/s, $\rho_s/\rho_f = 2.5$, and $h_T = h_R = 0.01$ m.

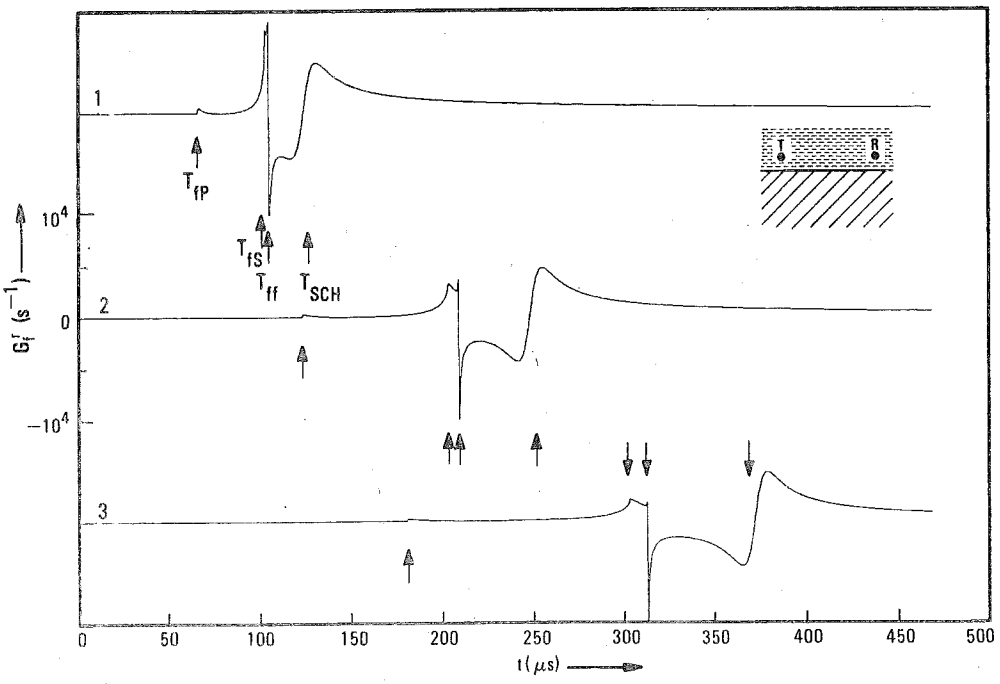

FIG. 4. Space–time Green's function G_f^r for the reflected acoustic pressure in a fluid from a fluid/solid interface as a function of time for three transmitter/receiver distances: (1) $d = 0.2$ m, (2) $d = 0.4$ m, (3) $d = 0.6$ m. Further, $c_P = 3500$ m/s, $c_S = 2000$ m/s, $c_f = 1920$ m/s, $\rho_s/\rho_f = 2.5$, and $h_T = h_R = 0.01$ m.

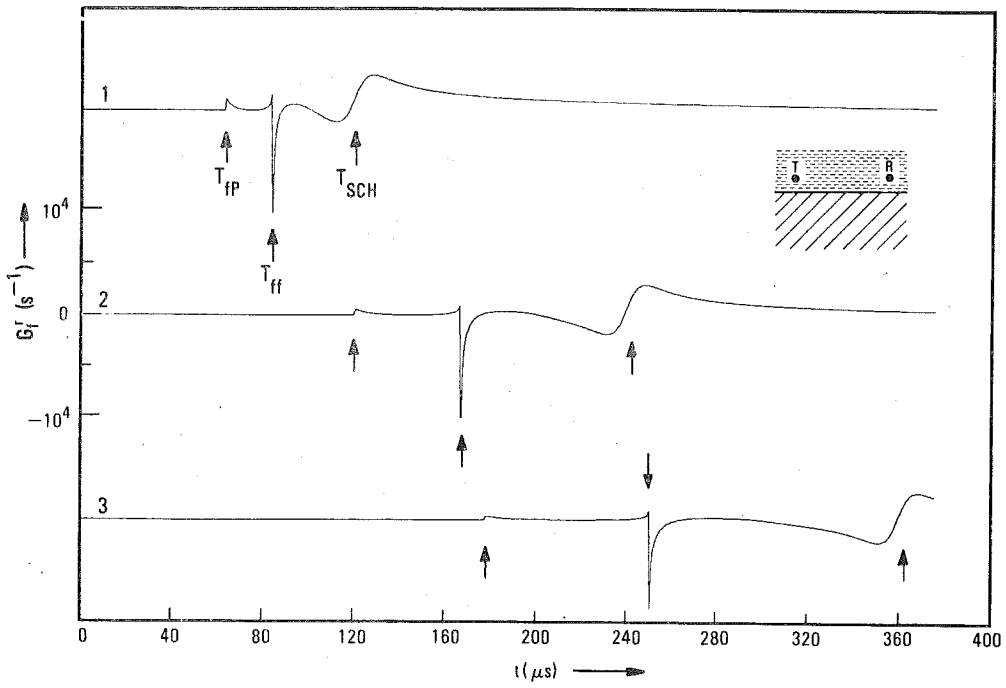

FIG. 5. Space–time Green's function G_f^r for the reflected pressure in a fluid from a fluid/solid interface as a function of time for three transmitter/receiver distances: (1) $d = 0.2$ m, (2) $d = 0.4$ m, (3) $d = 0.6$ m. Further, $c_P = 3500$ m/s, $c_S = 2000$ m/s, $c_f = 2400$ m/s, $\rho_s/\rho_f = 2.5$, and $h_T = h_R = 0.01$ m.

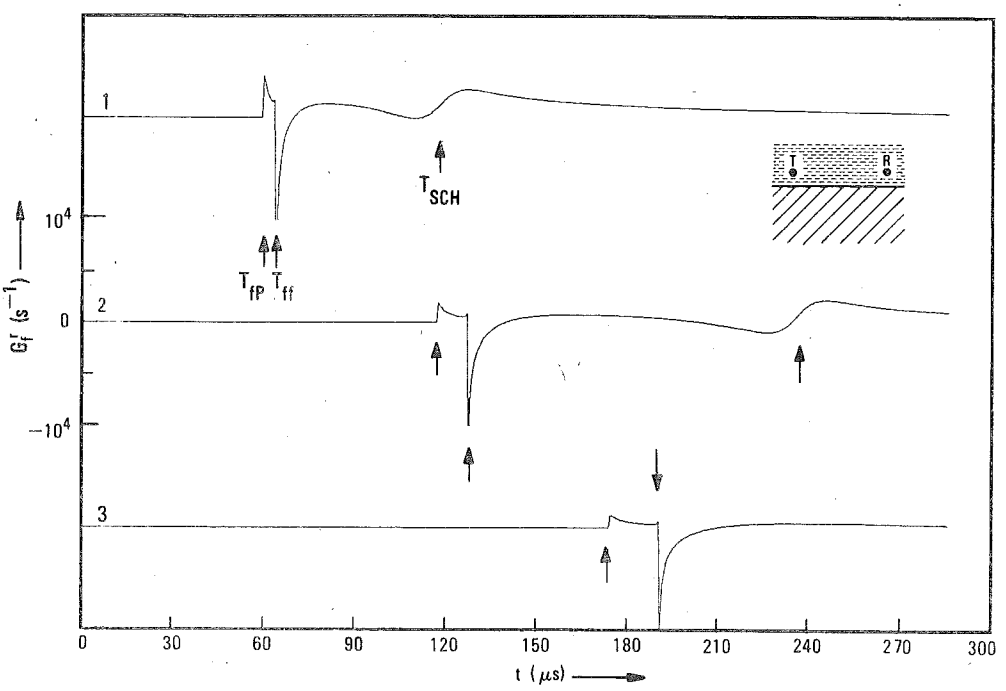

FIG. 6. Space–time Green's function G_f^r for the reflected pressure in a fluid from a fluid/solid interface as a function of time for three transmitter/receiver distances: (1) $d = 0.2$ m, (2) $d = 0.4$ m, (3) $d = 0.6$ m. Further, $c_P = 3500$ m/s, $c_S = 2000$ m/s, $c_f = 3150$ m/s, $\rho_s/\rho_f = 2.5$, and $h_T = h_R = 0.01$ m.

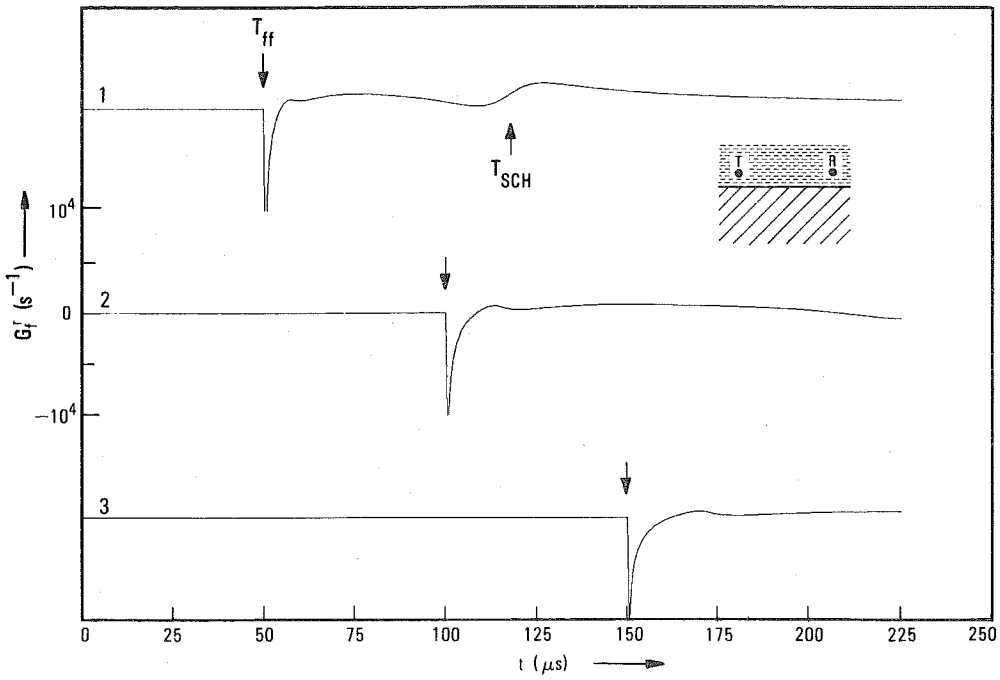

FIG. 7. Space–time Green's function G_f^r for the reflected acoustic pressure in a fluid from a fluid/solid interface as a function of time for three transmitter/receiver distances: (1) $d = 0.2$ m, (2) $d = 0.4$ m, (3) $d = 0.6$ m. Further, $c_P = 3500$ m/s, $c_S = 2000$ m/s, $c_f = 4000$ m/s, $\rho_s/\rho_f = 2.5$, and $h_T = h_R = 0.01$ m.

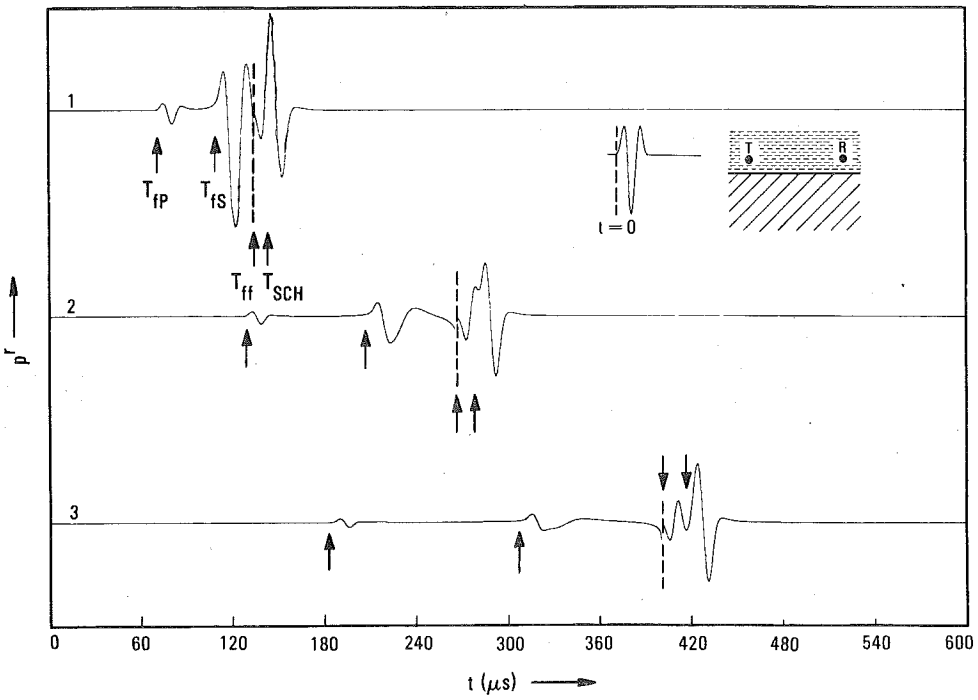

FIG. 8. Reflected acoustic pressure p^r in a fluid from a fluid/solid interface as a function of time for three transmitter/receiver distances: (1) $d = 0.2$ m, (2) $d = 0.4$ m, (3) $d = 0.6$ m. The pressure source pulse is also shown. Further, $c_P = 3500$ m/s, $c_S = 2000$ m/s, $c_f = 1500$ m/s, $\rho_s/\rho_f = 2.5$, and $h_T = h_R = 0.01$ m. The vertical scales for the signal prior to T_{ff} are ten times the vertical scales after T_{ff}. The source pulse duration $T = 20\,\mu$s.

in which the constants b_n are given by $b_0 = +0.35869$, $b_1 = -0.48829$, $b_2 = +0.14128$, and $b_3 = -0.01168$. The corresponding pressure source pulse, which is the second derivative of $\rho_f \phi_V(t)$ [see Eq. (32)] shows great similarity with the classical Ricker wavelet often used in seismology.

VI. CONCLUSION

With the aid of the modified Cagniard technique, a simple closed-form expression has been derived for the acoustic pressure in space–time of the wave that is reflected and refracted into the fluid when an impulsive, two-dimensional monopole line source is present near the plane interface between a fluid and a solid. Numerical results illustrate the different features that show up in the different regimes that exist for the wave speed in the fluid in relation to the wave speeds (compressional, shear, Rayleigh) in the solid. The numerical evaluation of the expressions requires much less time than would be the case for the analysis through the evaluation of the standard time–space Fourier inversion integrals.

APPENDIX: POLES AND ZEROS OF THE REFLECTION COEFFICIENT

In this Appendix we show, with the aid of the principle of the argument from complex function theory, that the fluid/solid reflection coefficient R_f has two poles and four zeros in the cut p plane as used to evaluate the space–time response in the configuration. Let

$$R_f = N_{\mathrm{SCH}}/\Delta_{\mathrm{SCH}}, \tag{A1}$$

where [cf. Eq. (26)]

$$N_{\mathrm{SCH}} = -\rho_f\gamma_P/4\rho_s\gamma_f\, c_S^4 + (p^2 - 1/2c_S^2)^2 + p^2\gamma_P\,\gamma_S \tag{A2}$$

and

$$\Delta_{\mathrm{SCH}} = \rho_f\gamma_P/4\rho_s\gamma_f\, c_S^4 + (p^2 - 1/2c_S^2)^2 + p^2\gamma_P\gamma_S. \tag{A3}$$

In accordance with our choice of the branches of the square-root expressions, both N_{SCH} and Δ_{SCH} are single valued in the cut p plane as shown in Fig. A1.

Let NPOLES denote the number of poles of R_f in the cut p plane and NZEROS the number of zeros, then the principle of the argument states that

$$\mathrm{NPOLES} = (2\pi i)^{-1}\left\{\int_{C_\infty} + \int_{L^+} + \int_{L^-}\right\}\left(\frac{\partial_p\,\Delta_{\mathrm{SCH}}}{\Delta_{\mathrm{SCH}}}\right)dp \tag{A4}$$

and

$$\mathrm{NZEROS} = (2\pi i)^{-1}\left\{\int_{C_\infty} + \int_{L^+} + \int_{L^-}\right\}\left(\frac{\partial_p\,N_{\mathrm{SCH}}}{N_{\mathrm{SCH}}}\right)dp. \tag{A5}$$

In Eqs. (A4) and (A5) we have used the property that both N_{SCH} and Δ_{SCH} remain bounded in the cut p plane. First, we calculate the contribution from C_∞, a circle with center at the origin and arbitrarily large radius. Since

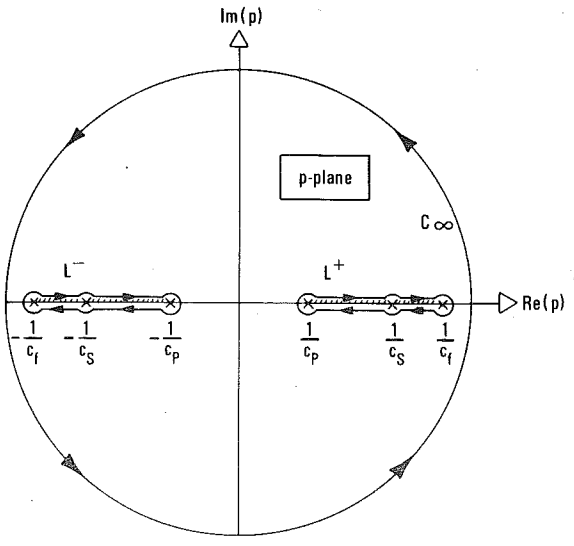

FIG. A1. The cut p plane and the contours used to determine the number of poles and zeros of the reflection coefficient.

$$\Delta_{\mathrm{SCH}} \sim -p^2(1/2c_S^2 - 1/2c_P^2) \text{ as } |p| \to \infty \tag{A6}$$

and

$$N_{\mathrm{SCH}} \sim -p^2(1/2c_S^2 - 1/2c_P^2) \text{ as } |p| \to \infty, \tag{A7}$$

we have

$$(2\pi i)^{-1}\int_{C_\infty}\left(\frac{\partial_p\,\Delta_{\mathrm{SCH}}}{\Delta_{\mathrm{SCH}}}\right)dp = (2\pi i)^{-1}\int_{C_\infty} 2p^{-1}\,dp = 2 \tag{A8}$$

and

$$(2\pi i)^{-1}\int_{C_\infty}\left(\frac{\partial_p\,N_{\mathrm{SCH}}}{N_{\mathrm{SCH}}}\right)dp = (2\pi i)^{-1}\int_{C_\infty} 2p^{-1}\,dp = 2. \tag{A9}$$

Further, upon substituting $p \to -p$, it easily follows that the contributions from the two loop integrals L^+ and L^- around the branch cuts are equal. Hence, it suffices to calculate the contribution from L^+ only. The contribution to L^+ consists of the contributions from the circular arcs C^P, C^S, and C^f around the branch points $p = 1/c_P$, $p = 1/c_S$, and $p = 1/c_f$, respectively, and the contribution from the remaining principal-value integrals. By using the local expansions

$$\partial_p\,\Delta_{\mathrm{SCH}}/\Delta_{\mathrm{SCH}} = O(\gamma_P^{-1}) \text{ as } p \to 1/c_P, \tag{A10}$$

$$\partial_p\,\Delta_{\mathrm{SCH}}/\Delta_{\mathrm{SCH}} = O(\gamma_S^{-1}) \text{ as } p \to 1/c_S, \tag{A11}$$

$$\partial_p\,\Delta_{\mathrm{SCH}}/\Delta_{\mathrm{SCH}} \sim p/\gamma_f^2 \text{ as } p \to 1/c_f, \tag{A12}$$

it follows that

$$(2\pi i)^{-1}\int_{C^P}\left(\frac{\partial_p\,\Delta_{\mathrm{SCH}}}{\Delta_{\mathrm{SCH}}}\right)dp \to 0, \tag{A13}$$

$$(2\pi i)^{-1}\int_{C^S}\left(\frac{\partial_p\,\Delta_{\mathrm{SCH}}}{\Delta_{\mathrm{SCH}}}\right)dp \to 0, \tag{A14}$$

$$(2\pi i)^{-1}\int_{C^f}\left(\frac{\partial_p\,\Delta_{\mathrm{SCH}}}{\Delta_{\mathrm{SCH}}}\right)dp = (2\pi i)^{-1}\int_{C^f}\left(\frac{p}{\gamma_f^2}\right)dp = 1/2. \tag{A15}$$

The principal-value integrals can be evaluated by observing that $\partial_p\,\Delta_{\mathrm{SCH}}/\Delta_{\mathrm{SCH}} = \partial_p[\ln(\Delta_{\mathrm{SCH}})]$. Their contributions all cancel except for the ones that arise from the end points near $p = 1/c_f$, for which we obtain

$$\begin{aligned}(2\pi i)^{-1}\lim_{\delta\downarrow 0}\{&\ln[\Delta_{\mathrm{SCH}}(1/c_f - \delta - i0)] \\ &- \ln[\Delta_{\mathrm{SCH}}(1/c_f - \delta + i0)]\} \\ &= (2\pi i)^{-1}\{-\pi i/2 - (\pi i/2)\} = -1/2.\end{aligned} \tag{A16}$$

Collecting the results, we arrive at

$$\mathrm{NPOLES} = 2. \tag{A17}$$

Now, checking the sign of Δ_{SCH} in the interval $1/c_f < \mathrm{Re}(p) < \infty$, $\mathrm{Im}(p) = 0$, we see that $\lim_{\delta\downarrow 0}\Delta_{\mathrm{SCH}}(1/c_f + \delta) = +\infty$, while $\Delta_{\mathrm{SCH}} \to -\infty$ as $p \to \infty$. Hence, one of the poles is located in the interval $1/c_f < \mathrm{Re}(p) < \infty$, $\mathrm{Im}(p) = 0$, the other in the interval $-\infty < \mathrm{Re}(p) < -1/c_f$, $\mathrm{Im}(p) = 0$. They are denoted by $p = \pm 1/c_{\mathrm{SCH}}$, respectively, where c_{SCH} is the speed of Scholte waves.

A similar analysis is carried out for N_{SCH}. By using the local expansions

$$\partial_p N_{\mathrm{SCH}}/N_{\mathrm{SCH}} = O(\gamma_P^{-1}) \text{ as } p \to 1/c_P, \tag{A18}$$

$$\partial_p N_{\mathrm{SCH}}/N_{\mathrm{SCH}} = O(\gamma_S^{-1}) \text{ as } p \to 1/c_S, \tag{A19}$$

$$\partial_p N_{\mathrm{SCH}}/N_{\mathrm{SCH}} \sim p/\gamma_f^2 \text{ as } p \to 1/c_f, \tag{A20}$$

it follows that,

$$(2\pi i)^{-1} \int_{C^P} \left(\frac{\partial_p N_{\mathrm{SCH}}}{N_{\mathrm{SCH}}}\right) dp \to 0, \tag{A21}$$

$$(2\pi i)^{-1} \int_{C^S} \left(\frac{\partial_p N_{\mathrm{SCH}}}{N_{\mathrm{SCH}}}\right) dp \to 0, \tag{A22}$$

$$(2\pi i)^{-1} \int_{C^f} \left(\frac{\partial_p N_{\mathrm{SCH}}}{N_{\mathrm{SCH}}}\right) dp = (2\pi i)^{-1} \int_{C^f} \left(\frac{p}{\gamma_f^2}\right) dp = 1/2. \tag{A23}$$

The principal-value integrals are again evaluated by using the property $\partial_p N_{\mathrm{SCH}}/N_{\mathrm{SCH}} = \partial_p [\ln(N_{\mathrm{SCH}})]$. Their contributions all cancel except for the ones that arise from the end points near $p = 1/c_f$, for which we obtain

$$\begin{aligned}(2\pi i)^{-1} \lim_{\delta \downarrow 0} &\{\ln[N_{\mathrm{SCH}}(1/c_f - \delta - i0)] \\ &- \ln[N_{\mathrm{SCH}}(1/c_f - \delta + i0)]\} \\ &= (2\pi i)^{-1}[i\pi/2 - (-i\pi/2)] = 1/2.\end{aligned} \tag{A24}$$

Collecting the results, we arrive at

$$\mathrm{NZEROS} = 4. \tag{A25}$$

The location of the zeros depends upon the parameter values of the two media.

The above analysis is correct, as long as there are no zeros on the branch cuts. It is easily verified that, on the branch cuts, the real and imaginary parts of Δ_{SCH} never vanish simultaneously. With N_{SCH} the situation is different. The real and imaginary parts of N_{SCH} vanish simultaneously if the condition "$\gamma_S \gamma_f$ is real and positive" is satisfied, and

$$p^2 - 1/2c_S^2 = 1, \tag{A26}$$

$$-\rho_f/\rho_s + 4c_S^4 \gamma_S \gamma_f = 0, \tag{A27}$$

simultaneously. These conditions can only be met if $1/2c_S^2 < 1/c_f^2$ and

$$\rho_f/\rho_s = (2c_S^2/c_f^2 - 1)^{1/2}. \tag{A28}$$

The zero is then located at $p = 1/2^{1/2}\, c_S$.

The zeros $p = \pm 1/2^{1/2}\, c_S$ can be regarded as double zeros in the sense that if Eq. (A28) is satisfied, nowhere else in the cut p plane zeros occur. This can, again, be verified by applying the principle of the argument. By observing that in the neighborhood of $p = \pm 1/2^{1/2}\, c_S$ we have N_{SCH} = (imaginary constant) $*$ $(p^2 - 1/2\, c_S^2)$, it follows that

$$\frac{\partial_p N_{\mathrm{SCH}}}{N_{\mathrm{SCH}}} = \frac{2p}{(p^2 - 1/2c_S^2)} \text{ if } \left|p^2 - \frac{1}{2c_S^2}\right| \to 0. \tag{A29}$$

Consequentlv, each of the four semicircular arcs around $p = \pm 1/2^{1/2}\, c_S$ contributes $-1/2$ to the argument integral. Finally, the remaining principal-value integrals around $p = \pm 1/2^{1/2}\, c_S$ contribute together $4 * (-1/2) = -2$. Collecting all results, it follows that no zeros are present in the cut p plane.

In general, the same type of proof leads to $c_{\mathrm{SCH}} < \min(c_f, c_R)$.

[1]W. L. Roever, T. F. Vining, and E. Strick, "Propagation of elastic wave motion from an impulsive source along a fluid/solid interface; I. Experimental pressure response; II. Theoretical pressure response; III. The pseudo-Rayleigh wave," Philos. Trans. R. Soc. (London), Ser. A **251**, 455–523 (1959).

[2]A. T. de Hoop, "A modification of Cagniard's method for solving seismic pulse problems," Appl. Sci. Res., Sec. B **8**, 349–356 (1960).

[3]A. T. de Hoop, "Theoretical determination of the surface motion of a uniform elastic half-space produced by a dilatational, impulsive, point source," Proceedings Colloques International C.N.R.S. No. 111, Marseille, 21–32 (1961) (in English).

[4]A. T. de Hoop, "Pulsed electromagnetic radiation from a line source in a two-media configuration," Radio Sci. **14**, 253–268 (1979).

[5]J. D. Achenbach, *Wave Propagation in Elastic Solids* (North-Holland, Amsterdam, 1973), p. 298.

[6]K. Aki and P. G. Richards, *Quantitative Seismology* (Freeman, San Francisco, 1980), p. 224.

[7]J. Miklowitz, *The Theory of Elastic Waves and Waveguides* (North-Holland, Amsterdam, 1978), p. 302.

[8]Lord Rayleigh, Proc. London Math. Soc. **17**, 4–11 (1887).

[9]J. D. Achenbach, *Wave Propagation in Elastic Solids* (North-Holland, Amsterdam, 1973), p. 187.

[10]J. G. Scholte, "On the large displacements commonly regarded as caused by Love waves and similar dispersive surface waves," Proc. K. Ned. Akad. Wet. **51**, 533–543, 642–649, 828–835, 969–976 (1948) (in English).

[11]J. G. Scholte, "On true and pseudo Rayleigh waves," Proc. K. Ned. Akad. Wet. **52**, 652–653 (1949) (in English).

[12]L. Cagniard, *Reflection and Refraction of Progressive Seismic Waves* (McGraw–Hill, New York, 1962), p. 245. [Translation and revision of L. Cagniard, *Reflexion et Refraction des Ondes Seismiques Progressives* (Gauthier-Villars, Paris, 1939) by E. A. Flinn and C. H. Dix.]

[13]J. Miklowitz, *The Theory of Elastic Waves and Waveguides* (North-Holland, Amsterdam, 1978), p. 168.

[14]D. V. Widder, *The Laplace Transform* (Princeton U. P., Princeton, NJ, 1946), p. 63.